

Insight into the Characterization of Sea-Salt Batteries

Kouwerberg, Sang Jae; Alpizar Castillo, J.J.; Ramirez Elizondo, L.M.; Bauer, P.

DOI

[10.1109/CPE-POWERENG58103.2023.10227412](https://doi.org/10.1109/CPE-POWERENG58103.2023.10227412)

Publication date

2023

Document Version

Final published version

Published in

2023 IEEE 17th International Conference on Compatibility, Power Electronics and Power Engineering (CPE-POWERENG)

Citation (APA)

Kouwerberg, S. J., Alpizar Castillo, J. J., Ramirez Elizondo, L. M., & Bauer, P. (2023). Insight into the Characterization of Sea-Salt Batteries. In *2023 IEEE 17th International Conference on Compatibility, Power Electronics and Power Engineering (CPE-POWERENG)* (pp. 1-6). IEEE. <https://doi.org/10.1109/CPE-POWERENG58103.2023.10227412>

Important note

To cite this publication, please use the final published version (if applicable).
Please check the document version above.

Copyright

Other than for strictly personal use, it is not permitted to download, forward or distribute the text or part of it, without the consent of the author(s) and/or copyright holder(s), unless the work is under an open content license such as Creative Commons.

Takedown policy

Please contact us and provide details if you believe this document breaches copyrights.
We will remove access to the work immediately and investigate your claim.

Green Open Access added to TU Delft Institutional Repository

'You share, we take care!' - Taverne project

<https://www.openaccess.nl/en/you-share-we-take-care>


Otherwise as indicated in the copyright section: the publisher is the copyright holder of this work and the author uses the Dutch legislation to make this work public.

Insight into the Characterization of Sea-Salt Batteries


Sang Jae Kouwenberg

DC Systems, Energy Conversion & Storage
Delft University of Technology
Delft, The Netherlands
D.S.J.Kouwenberg@student.tudelft.nl


Joel Alpízar-Castillo

DC Systems, Energy Conversion & Storage
Delft University of Technology
Delft, The Netherlands
J.J.AlpizarCastillo@tudelft.nl 

Laura Ramírez-Elizondo

DC Systems, Energy Conversion & Storage
Delft University of Technology
Delft, The Netherlands
L.M.RamirezElizondo@tudelft.nl 

Pavol Bauer

DC Systems, Energy Conversion & Storage
Delft University of Technology
Delft, The Netherlands
P.Bauer@tudelft.nl 

Abstract—Batteries are one of the main tools to provide the flexibility distribution and transmission systems need due to their increasing dependence on weather conditions. However, environmental and economic factors pose a significant problem. New types of batteries that do not rely on rare earth metals and organic solvents but instead use water and more common ions could be a cost-effective and environmentally safe way to provide energy storage in the future. We studied the performance of sea-salt cells designed as a low-cost, environmentally friendly method to store electricity. We used a constant current charge/discharge test with different currents, from 50 mA to 300 mA, to identify the maximum efficiencies of the cell. Then, we introduced a new strategy to determine the cut-off voltage to discharge the battery, inspired by the maximum power point found in photovoltaics. We used a constant voltage charge to determine the cell's energy density. However, evidence of side reactions urged us to use constant current charge/discharge tests to identify the battery's capacity based on the efficiencies drop. Results showed a maximum energy efficiency of 74.6% at 200 mA and a maximum Coulombic efficiency of 88.7% at 300 mA. The cut-off voltage of the cell during discharge should be between 1.4 V and 1.6 V. The energy densities range from 10.1 Wh/kg (6.53 Wh/L) with an efficiency of 57.5% and 4.18 Wh/kg (2.7 Wh/L) with an efficiency of 69.8%.

Index Terms—Energy storage, Sea-salt battery, Zn battery

I. INTRODUCTION

The widespread usage of fossil fuels to shape and power modern society has lead to a slow but inevitable rise in global average temperatures and associated changes in climate. Measurements on global temperatures have shown a 1.04 °C increase since pre-industrial times, with an average increase of 0.14 °C per decade since 1981 [1]. In response, several international climate accords have been signed. The most

The project was carried out with a Top Sector Energy subsidy from the Ministry of Economic Affairs and Climate, carried out by the Netherlands Enterprise Agency (RVO). The specific subsidy for this project concerns the MOOI subsidy round 2020. Thanks to Dr. Ten B.V. (developer of the technology) for providing a sample of their developed cells for the experiments.

recent Paris Agreement was signed in 2016 by a record 197 signatories, striving to reduce greenhouse gas emissions by 50% by 2030 and to limit the global temperature rise to 2 °C above pre-industrial levels. While these accords and agreements have had little direct impact on the total amount of emissions thus far, they have had a significant knock-on effect on the research and development of renewable energy sources via subsidies, emission taxes and other schemes.

For instance, in the Netherlands, a combination of the European Emission Trading Scheme [2], and subsidies for renewable energy and energy-saving measures [3] have made it increasingly attractive from an economic perspective for both businesses and individuals to dive into renewable energy. The effects of these measures are clearly visible in the amount of installed capacity for renewable energy sources. Only solar energy boasts over 1.7 million installations, indicating a potentially sizeable contribution of individual homeowners and micro-installations [4], [5]. However, this has had an unfortunate side effect on the Dutch grid; coupled with the increased electrification of heating and transportation, both the transmission and distribution grids are quickly reaching maximum capacity. As of June 2022, almost half of the distribution network managed by Liander has no spare capacity [6]. In mid-July, Tennet announced that no new large-scale users could connect to the transmission grid in provinces Noord Brabant and Limburg [7]. Additional capacity would solve this problem in the short term, but a different solution would be needed to ensure power balance stability in the long term.

Maintaining the balance between power production and consumption is among the biggest challenges of any grid. This is usually done by gas-powered generators, as they can ramp up and down rapidly within short time frames (on the order of several minutes). Adding renewable energy into the energy mix increases the balancing complexity [8]. Reshaping the energy grid to form microgrids could increase the grid flexi-

bility without a forced overbuilding capacity. The transmission networks would require less capacity by allocating generators closer to the loads, as most of the demand can be fulfilled by nearby sources. This also increases overall efficiency; shorter cables mean less power loss and decreased reactive power needs, depending on whether the microgrid operates using AC or DC voltage [9]. Additionally, microgrids can provide ancillary services to the distribution system operator. This can be done on any time scale, depending on the technology [10]; however, current trends heavily depend on battery energy storage systems as the technology that can provide more ancillary services [11].

Lithium-ion batteries are the most common battery type. They boast high specific energy, specific power, and efficiency, making them a prime candidate for a wide variety of applications, from portable electronics to large-scale power storage [12]. They are also lighter than other battery technologies and have a very low self-discharge. They are, however, expensive to produce due to the scarcity of the required materials and might become an environmental issue if they are not appropriately handled after their end of life. Therefore, more environmentally friendly chemistries should be investigated since energy storage is a fundamental component of microgrids.

Previous works regarding room-temperature operating salt batteries show the challenges to face before including this technology on the market as an alternative to Lithium-ion batteries. The main challenges are related to maintaining the efficiencies and capacity of the battery stable during its life. In [13], after 100 cycles, the battery retained 80% of its initial capacity and only 60% after 200 cycles. More recently, [14] achieved a Coulombic efficiency of 84% after 1 500 cycles. Similarly, [13] reported capacities below 60 mAh·g⁻¹, although capacities up to 300 mAh·g⁻¹ were reported by [15] for lifetimes below 100 cycles.

In this work, we evaluated the properties of a more recent sea-salt battery prototype than the one described in [16] as an alternative to lithium-ion. This rechargeable zinc-based battery is composed of chemicals with a low GHS hazard rating, as shown in Table I (note that the last two entries and the concentrations of the electrolyte's components are not specified, as these are company confidential). During the operation, there are two main intermediates formed: metallic zinc (solid), and an aqueous complex of carbon, chloride, and bromide (C-Br_xCl_y). Previous research highlights some advantages of the battery, mostly on its low cost and environmentally friendly construction [16]. On the other hand, work still needs to be done to characterize the behavior and efficiency of the battery under different loads. Therefore, the contributions of this paper are towards identifying the energy and charge efficiencies of the battery and how different load conditions influence its performance. Additionally, we proposed a method to control the cut-off voltage during the discharge of the battery, based on the maximum power point used in photovoltaics, as commercially available inverter technologies are not yet designed to operate with the sea-salt battery.

TABLE I: Components used in the sea-salt battery and their GHS hazard classification [16].

Component	Role	Hazard
<i>Electrode</i>		
Treated graphite plate	Anode/Cathode	None
Treated graphite felt	Anode/Cathode	None
<i>Electrolyte</i>		
Water	Solvent	None
NaCl (aq)	Main component	None
ZnCl ₂ (aq)	Main component	Warning, corrosive Danger to aquatic life
NaBr (aq)	Main component	None
ZnBr ₂ (aq)	Main component	Warning, corrosive, danger to aquatic life Corrosive
AlCl ₃ (aq)	Catalyst	Warning
MgBr ₂ (aq)	Dendrite prevention agent	Warning
Amine complexes	Stabilizer	n/a
Organic surfactants	Stabilizer	n/a

II. CONSTANT CURRENT CHARGE/DISCHARGE TEST

The measured battery was provided by the manufacturer. It consists of 4 cells (0.16 L and 0.1 kg each), connected in parallel by threaded graphite rods, capped with graphite nuts. A ring-style wire-end connector was added to each electrode to provide a connection point. The battery was controlled using an Arbin LBT 22043 battery tester. Following the manufacturer's recommendations, the control cycle was as follows: first, the battery was charged at 200 mA for 7 hrs (1.4 Ah), then let to rest for 1 h, and finally, it was discharged at 200 mA until the voltage dropped to 0 V. To evaluate how the battery performs under different load conditions, we charged the battery with capacities from 0.8 Ah to 1.4 Ah with different currents, as shown in Table II. The rest period was one hour for all cases, and the discharge current was the same as the charging current.

The overall voltage behavior during charge, rest, and discharge is consistent with [16]. During the charge, the curves start with a sharp increase in voltage, which proceeds to level out between 1.75 V and 1.9 V, where the higher the charging current, the higher the final voltage (see Fig. 1). The discharge curves follow the same pattern in reverse, with the voltage remaining mostly constant with a sharp decrease towards the end of the measurement, where the higher the discharging current, the lower the initial voltage (see Fig. 2). The slope is proportional to the current in both cases, at the start of the charge and at the end of the discharge.

Tables III and IV show the maximum energy and Coulombic efficiencies for the primary measurements from full charge to full discharge, color-coded from lowest (blue) to highest (red). Coulombic efficiency shows a clear trend. Applying higher currents to the battery increases Coulombic efficiency from below 70% at 50 mA to above 80% at 300 mA. On the other hand, energy efficiency results show a maximum at 200 mA. For both efficiencies, shorter charging times caused better results than longer charging times.

To understand how the efficiency changes with the battery's aging, we repeated the control cycle (charge the battery for 7

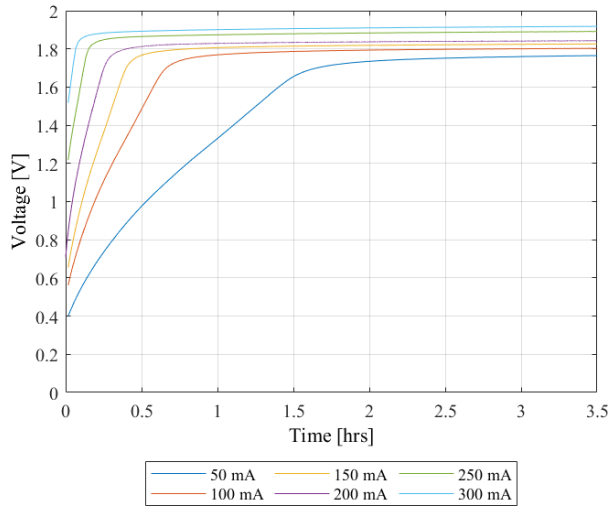


Fig. 1: Charging voltage curves at each applied current during the 1.12 Ah test up until 3.5 hrs. The initial rate of voltage increase correlates to the amount of current used, as does the final voltage. Some measurements did take longer but are not fully shown for the purpose of this graph.

TABLE II: The total charge time in hours for each charge step, for each applied current and total charge.

Current	Total charge			
	0.8 Ah	0.93 Ah	1.12 Ah	1.4 Ah
50 mA	16	18	22	28
100 mA	8	9	11	14
150 mA	5	6	7	9
200 mA	4	4.67	5.6	7
250 mA	3.2	3.75	4.5	5.6
300 mA	2.6	3.1	3.75	4.6

hrs, let it rest for one hour, and discharge it until 0 V) 25 times, with a rest period of one hour between cycles. The results showed a 10% drop in energy efficiency and a 26% drop in Coulombic efficiency. Despite our results being consistent with the literature regarding the accelerated aging of room-temperature salt-based batteries [13], [17], [18], previous work done by [16] suggested more optimistic efficiency values with this specific battery. The experiment done by [16] consisted of 1400 cycles of 50 mAh charge, resulting in a maximum Coulombic efficiency of 94% with a total drop of 22% and a maximum energy efficiency of 65.5% with a 34% drop.

The difference between our results and the reported by [16] can be explained as there are three main differences between the experiments:

- 1) *The current*: [16] used 50 mA in a single cell, whereas we tested a battery composed of four cells. In this sense, the current per cell would be approximately 50 mA; nevertheless, when grouping cells, a drop in efficiency is expected.

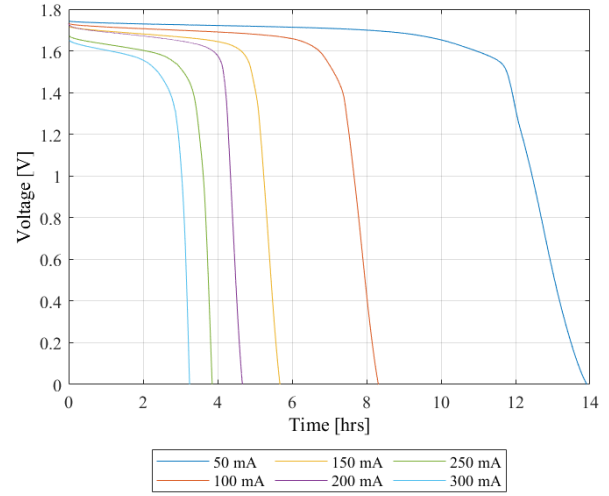


Fig. 2: Representative discharging voltage curves at each applied current during the 1.12 Ah test. The voltage drops at the end of each measurement have almost identical slopes except for the 50 mA measurement. At higher applied currents (250, 300 mA), the initial near-constant voltage region all but disappears.

TABLE III: Coulombic efficiencies for all experiments, expressed in percentages. Note the increase in efficiency with increasing current and decreasing charge.

Charge [Ah]	Current [mA]					
	50	100	150	200	250	300
1.4	58.87	72.14	77.86	80.02	82.83	83.85
1.12	63.23	75.60	81.06	83.31	85.65	86.61
0.93	67.71	78.43	82.51	85.86	86.77	88.33
0.8	69.54	79.89	84.09	87.30	87.61	88.73

- 2) *The charge*: even though our base scenario (1.4 Ah) was recommended by the manufacturer, the results shown in the Tables III and IV suggest that shorter cycles would result in better performances. If a linear behavior is assumed between the efficiencies and the time, when extrapolating our results to charge cycles of 1 h, the Coulombic efficiency ranges from 80% to 90%, and the energy efficiency ranges from 70% to 80%. In both cases, the maximum value is obtained at 200 mA.
- 3) *The cut-off voltage*: the experiment done by [16] stopped the discharge at 0.7 V. As we intend to create the full voltage curve, we discharged until 0 V. As expected, discharging the battery further the optimal discharge voltage can decrease the efficiency, as it accelerates the aging of the battery. However, this voltage has not been identified by [16] nor by the manufacturer of the battery.

III. MAXIMUM VOLTAGE-TIME POINT

The tests detailed in Section II discharged the battery until 0 V to obtain the complete voltage curves; however, a cut-off voltage during discharge is required to avoid accelerating the

TABLE IV: Energy efficiencies for all measurements, expressed in percentage points. Note the maximum at 0.8 Ah and 200 mA.

Charge [Ah]	Current [mA]					
	50	100	150	200	250	300
1.4	52.04	63.90	67.94	69.78	67.20	65.13
1.12	56.14	66.84	70.34	71.93	68.88	67.20
0.93	59.67	68.81	71.15	73.93	69.50	68.11
0.8	61.03	69.74	71.98	74.60	69.90	68.26

battery's aging. In this work, we introduced a new method to determine such point for the sea-salt battery. The method is inspired by the maximum power point estimation in photovoltaics, given the resemblance of the voltage curve during the discharge of the battery to the I-V curve. We calculated the product of voltage and discharge time per measurement and plotted it as a function of time. The resulting curve is similar to the power curve from a PV cell, as shown in Fig. 5. Thus, we calculated the maximum of the voltage-time curve, called the maximum voltage-time point (MVTP), obtaining the corresponding voltage in the voltage curve.

To evaluate the method's suitability, we calculated the MVTP for each of the charge conditions presented in Table II for a battery comprised of four cells in parallel. Additionally, we tested three cells with a charge current of 50 mA and the same discharge times indicated for the 200 mA test in Table II. For all cycles, the discharge was stopped once the voltage dropped to 0 V. The results demonstrate that the MVTP consistently remains near 90% of the total energy if the battery was to be discharged until 0 V for both the cells (see Fig. 3) and the battery (see Fig. 4). This behavior is consistent independently of the discharged energy or the discharge current.

When calculating the MVTP, the cut-off voltage was consistent per current. However, the voltages do not seem to follow a trend based on the applied current levels. At lower currents, the voltages at the MVTP are around 1.57 V from 50 mA up to 200 mA. At 250 mA and 300 mA, however, the MVTP voltage drops significantly down to 1.44 V and 1.39 V, respectively. Fig. 6 shows the MVTP voltages for the repeated measurements, with the points in the graphs being in the order in which the measurements took place. There seems to be no significant correlation between the order in which the measurements are done and the resulting MVTP voltage. Given the above, a control strategy based on a fixed cut-off voltage might not be as effective as in other battery technologies. With the MVTP method, on the other hand, it is possible to implement a control strategy to stop the discharge of the battery.

IV. CONSTANT VOLTAGE CHARGE - CONSTANT CURRENT DISCHARGE TEST

Generally, the charging phase for a battery consists of two parts a constant current period and a constant voltage period [19]. This charging scheme is known as constant current

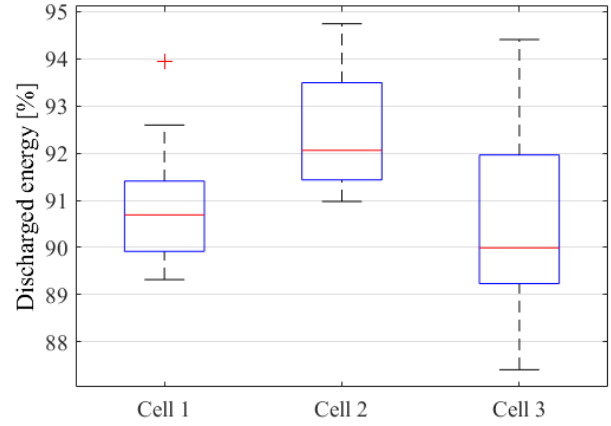


Fig. 3: Distribution of energy discharged from the cells until the MVTP, normalized against the total energy discharged until 0 V, at 50 mA.

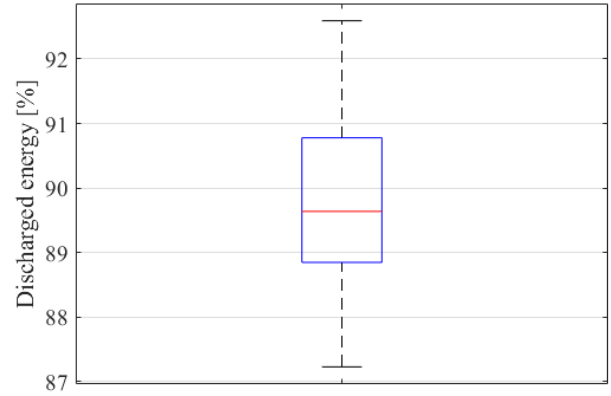


Fig. 4: Distribution of energy discharged from the battery until the MVTP, normalized against the total energy discharged until 0 V.

constant voltage (CCCV) charging. The general charging behavior of batteries is as follows: a constant current is injected into the battery, so its voltage rises as the SoC increases, followed by a region where the voltage remains near-constant. As the SoC approaches 1, the voltage spikes, indicating that the battery is fully saturated. At this moment, a constant voltage charge would cause the current to drop sharply, followed by a steady state region in which the current remains constant, then drop further to zero as the voltage of the battery exceeds the voltage of the measuring equipment.

A set of measurements was conducted at a constant voltage to find the battery's maximum capacity to validate the charge recommended by the manufacturer. The battery was first left to rest for 10 minutes. The intent was to follow the previous scheme, charging the battery at 1.8 V until the current reached

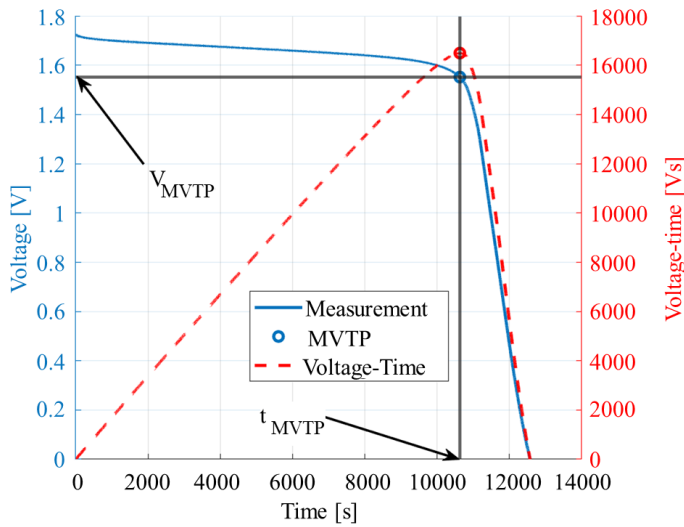


Fig. 5: Voltage and voltage-time curves during a constant current discharge, indicating the MVTP.

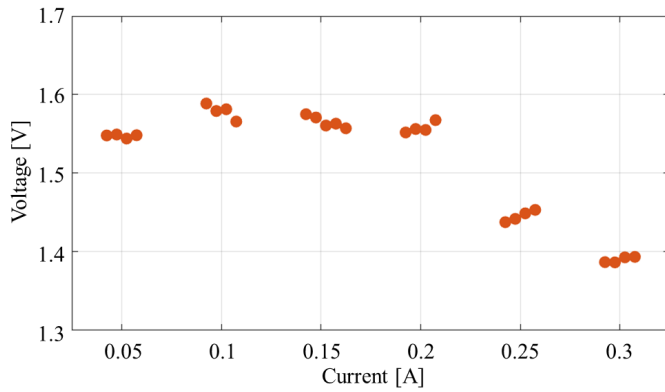


Fig. 6: The MVTP voltages at each applied current. The data points per applied current level are in chronological order.

0 A. However, as shown in Fig. 7, while the measurement proceeds through time, the current does not drop to 0 A. Instead, the current trends to a steady state level. Considering the data, the decision was made to cut the charge phase when the change in current approached 0 A/s. Due to software limitations, this had to be done manually. The battery was then left to rest for one hour. Then, it was discharged at 150 mA until 0 V. Finally, the battery was left to rest for one hour. This cycle was repeated three times in total.

While the initial fall in current takes the same time for each measurement, the rate of subsequent decay differs. The first measurement decayed the quickest, and the last decayed the slowest. The approximate value it trends towards differs too in each measurement; the first cycle ends the lowest at 100 mA, while the second and third cycles seem to trend towards 120 mA, though over different time spans. The extent to which the charge phase was allowed to continue also did not correlate strongly with the total discharge time. While the longer charge phase cycle also took longer to discharge, the difference in

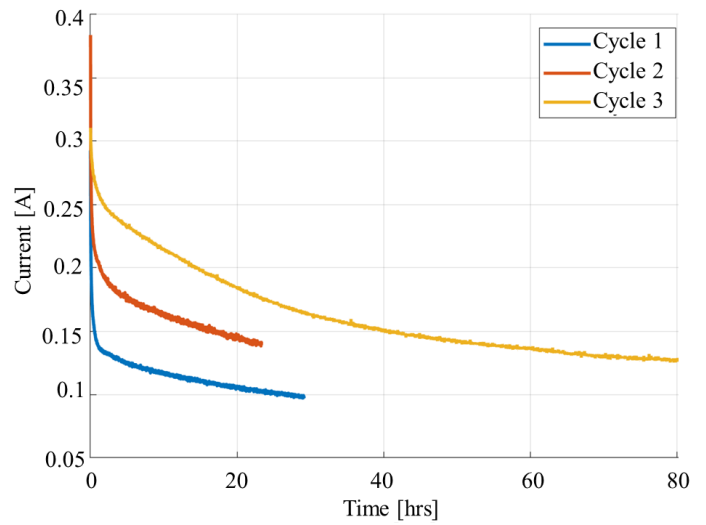


Fig. 7: Constant voltage charge curves. The current, despite dropping over time, did not reach 0 A, causing the charge phase to have to be ended manually.

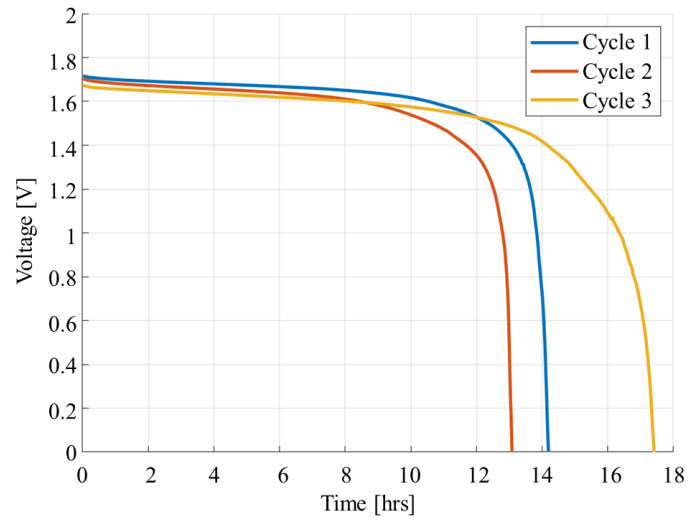


Fig. 8: Discharge phases for the constant voltage charge measurements. Note that these were performed under a constant current of 150 mA.

duration was not nearly as great as the difference between charge phase durations. The longer charge phase does seem to alter the physical processes somewhat, as the cycle with the longest charge phase sees a change in the discharge behavior towards lower SoC values. Instead of the sharp voltage drop, it seems to decrease over a longer period, without the more sudden onsets of the previous two cycles or any of the other measurements, as shown in Fig. 8. A summary of the charge and discharge results is presented in Table V.

These findings indicate that while the battery may have a stated capacity, the constant voltage charging method for determining the maximum capacity is unsuitable. Most likely, there is some form of side-reaction taking place inside the

TABLE V: Results of the constant voltage charge test.

	Cycle 1	Cycle 2	Cycle 3
Charge injected (Ah)	3.32	3.38	13.33
Charge extracted (Ah)	2.13	2.61	5.23
Coulombic efficiency (%)	64.2	68.1	39.2
Energy injected (Wh)	6.09	7.13	25.2
Energy extracted (Wh)	3.39	4.1	7.73
Energy efficiency (%)	55.7	57.5	30.9

battery that absorbs all the power once the battery approaches full capacity, which furthermore happens to have the same energy barrier that the electrical conversion of the active species has. The results suggest that the ideal amount of energy stored lies near cycles 2 and 3. Yet, the efficiencies obtained were lower than the tests with less charge, so a tradeoff between charge and efficiency should be considered.

V. CONCLUSIONS

We studied the performance of a sea-salt cell prototype, designed as a low-cost, environmentally friendly method to store electricity. We made a constant current charge/discharge test with different currents, from 50 mA to 300 mA. The maximum energy efficiency found was 74.6% at 200 mA, and the maximum Coulombic efficiency was 88.7% at 300 mA. However, we found drops of 10% in energy efficiency and 26% in charge efficiency after 25 cycles. We introduced a new strategy to determine the cut-off voltage to discharge the battery, inspired by the maximum power point in photovoltaics. The results suggest that the cut-off voltage of the cell should be between 1.4 V and 1.6 V, depending on the discharge conditions, which is a broad range. Instead, if the MVTP method is used, the discharge can remain consistently around 90% of the total energy when compared to a discharge up to 0 V. To determine the battery's maximum capacity and, therefore, its energy density, we used a constant voltage charge test, achieving an energy density of 10.1 Wh/kg, or 6.53 Wh/L with an efficiency of 57.5%. Nevertheless, the results suggest the existence of side reactions that made the current trend to values between 100 mA and 120 mA instead of 0 mA. On the other hand, if we considered the results from the constant current charge/discharge tests to identify the battery's capacity, based on the efficiencies drop, the battery's energy density is 4.18 Wh/kg, or 2.7 Wh/L, with an efficiency of 69.8%.

For the upcoming prototypes of this cell, we recommended repeating the experiments with a larger sample of cells to enhance the statistical validity of the values found for the battery's properties. We would also recommend elaborating on understanding the side reactions within the battery that avoid the constant voltage charge test reaching 0 A. This would provide insight into how one can detect when the reaction that charges the battery ends and the parasitic reaction takes over. Also, understanding if this reaction is reversible and if the presence of the products of this reaction interferes with the performance of the battery would be crucial to improve the performance of the battery. Finally, studies dedicated to

characterizing the aging of the battery would be useful to identify applications suitable for this technology.

REFERENCES

- [1] NOAA. (2022) NOAA National Centers for Environmental Information, State of the Climate: Monthly Global Climate Report for Annual 2021, published online January 2022. [Online]. Available: <https://www.ncei.noaa.gov/access/monitoring/monthly-report/global/202113>
- [2] European Commission, "EU emissions trading scheme," *EM: Air and Waste Management Association's Magazine for Environmental Managers*, no. FEB., pp. 10–11, 2008. [Online]. Available: https://climate.ec.europa.eu/eu-action/eu-emissions-trading-system-eu-ets_en
- [3] Mathias de Glad. (2023) Subsidies en regelingen voor verduurzaming. [Online]. Available: <https://www.kvk.nl/advies-en-informatie/innovatie/duurzaam-ondernemen/subsidies-en-regelingen-voor-vergroening/>
- [4] CBS. (2022) Renewable electricity; production and capacity. [Online]. Available: <https://www.cbs.nl/en-gb/figures/detail/82610ENG>
- [5] CBS. (2021) Green electricity production up by 40 percent. [Online]. Available: <https://www.cbs.nl/en-gb/news/2021/08/green-electricity-production-up-by-40-percent>
- [6] Liander. (2022) Beschikbaarheid capaciteit. [Online]. Available: <https://www.liander.nl/grootzakelijk/transportschaarste/beschikbaarheid-capaciteit>
- [7] TenneT. (2022) Voorlopige stop voor nieuwe grootverbruikers van elektriciteit noord-brabant en limburg. [Online]. Available: <https://www.tennet.eu/nl/nieuws/voorlopige-stop-voor-nieuwe-grootverbruikers-van-energie-nord-brabant-en-limburg>
- [8] J. Alpi zar-Castillo, "Simplified model to approach the theoretical clear sky solar pv generation curve through a gaussian approximation," *Nigerian Journal of Technology*, vol. 40, pp. 44–48, 3 2021.
- [9] A. Mittal, A. Rajput, K. Johar, and R. Kandari, *Microgrids, their types, and applications*. INC, 2022. [Online]. Available: <http://dx.doi.org/10.1016/B978-0-323-85463-4.00008-3>
- [10] M. Geraedts, J. Alpi zar-Castillo, L. Ram rez-Elizondo, and P. Bauer, "Optimal sizing of a community level thermal energy storage system," in *2022 IEEE 21st Mediterranean Electrotechnical Conference (MELECON)*, 2022, pp. 52–57.
- [11] J. Alpi zar-Castillo, L. Ram rez-Elizondo, and P. Bauer, "Assessing the role of energy storage in multiple energy carriers toward providing ancillary services: A review," *Energies*, vol. 16, no. 1, 2023. [Online]. Available: <https://www.mdpi.com/1996-1073/16/1/379>
- [12] B. Sund n, "Battery technologies," *Hydrogen, Batteries and Fuel Cells*, pp. 57–79, 2019.
- [13] S. T. Senthilkumar, M. Abirami, J. Kim, W. Go, S. Min, and Y. Kim, "Sodium-ion hybrid electrolyte battery for sustainable energy storage applications," *Journal of Power Sources*, vol. 341, pp. 404–410, 2017. [Online]. Available: <http://dx.doi.org/10.1016/j.jpowsour.2016.12.015>
- [14] H.-s. Yang, M.-w. Park, K.-h. Kim, O. Lun, T.-i. Jeon, and J. Kang, "Facile in situ synthesis of dual-heteroatom-doped high-rate capability carbon anode for rechargeable seawater-batteries," *Carbon*, vol. 189, pp. 251–264, 2022. [Online]. Available: <https://doi.org/10.1016/j.carbon.2021.12.066>
- [15] D. Lim, C. Dong, H. W. Kim, G. Bae, K. Choo, G. Cho, Y. Kim, B. Jin, and J. Kim, "Redox chemistry of advanced functional material for low-cost and environment-friendly seawater energy storage," *Materials Today Energy*, vol. 21, p. 100805, 2021. [Online]. Available: <https://doi.org/10.1016/j.mtener.2021.100805>
- [16] B. Homan, "Batteries in Smart Microgrids," Ph.D. dissertation, University of Twente, 2020. [Online]. Available: <https://research.utwente.nl/en/publications/batteries-in-smart-microgrids>
- [17] J.-k. Kim, E. Lee, H. Kim, C. Johnson, and J. Cho, "Rechargeable Seawater Battery and Its Electrochemical Mechanism," *Chemelectrochem*, vol. 60439, pp. 328–332, 2015.
- [18] L. Wei, L. Zeng, M. C. Wu, X. Z. Fan, and T. S. Zhao, "Seawater as an alternative to deionized water for electrolyte preparations in vanadium redox flow batteries," *Applied Energy*, vol. 251, no. November 2018, 2019.
- [19] M. Nizam, H. Maghfiroh, B. Irfani, I. Inayati, and A. Ma'arif, "Designing and prototyping of lithium-ion charging system using multi-step constant current method," *World Electric Vehicle Journal*, vol. 13, no. 10, 2022. [Online]. Available: <https://www.mdpi.com/2032-6653/13/10/178>